

# High Sensitivity Array Observations of the $z = 1.87$ Sub-Millimeter Galaxy GOODS 850–3<sup>1</sup>

Emmanuel Momjian

*National Radio Astronomy Observatory, P. O. Box O, Socorro, NM, 87801, USA*

emomjian@nrao.edu

Wei-Hao Wang<sup>a</sup>

*Academia Sinica Institute of Astronomy and Astrophysics, P.O. Box 23-141, Taipei 10617,  
Taiwan*

whwang@asiaa.sinica.edu.tw

Kirsten K. Knudsen

*Argelander-Institut für Astronomie, Auf dem Hügel 71, D-53121 Bonn, Germany*

knudsen@astro.uni-bonn.de

Christopher L. Carilli

*National Radio Astronomy Observatory, P. O. Box O, Socorro, NM, 87801, USA*

ccarilli@nrao.edu

Lennox L. Cowie

*Institute for Astronomy, University of Hawaii, 2680 Woodlawn Drive, Honolulu, HI 96822,  
USA*

cowie@ifa.hawaii.edu

Amy J. Barger<sup>b,c</sup>

*Department of Astronomy, University of Wisconsin-Madison, 475 North Charter St.,  
Madison, WI 53706*

barger@astro.wisc.edu

---

<sup>a</sup>National Radio Astronomy Observatory, P. O. Box O, Socorro, NM, 87801, USA

## ABSTRACT

We present sensitive phase-referenced VLBI results on the radio continuum emission from the  $z = 1.87$  luminous submillimeter galaxy (SMG) GOODS 850–3. The observations were carried out at 1.4 GHz using the High Sensitivity Array (HSA). Our sensitive tapered VLBI image of GOODS 850–3 at  $0.47'' \times 0.34''$  ( $3.9 \times 2.9$  kpc) resolution shows a marginally resolved continuum structure with a peak flux density of  $148 \pm 38 \mu\text{Jy beam}^{-1}$ , and a total flux density of  $168 \pm 73 \mu\text{Jy}$ , consistent with previous VLA and MERLIN measurements. The deconvolved size of the source is  $0''.27(\pm 0''.12) \times < 0''.23$ , or  $2.3(\pm 1.0) \times < 1.9$  kpc<sup>2</sup>, and the derived intrinsic brightness temperature is  $> (5 \pm 2) \times 10^3$  K. The radio continuum position of this galaxy coincides with a bright and extended near-infrared source that nearly disappears in the deep HST optical image, indicating a dusty source of nearly 9 kpc in diameter. No continuum emission is detected at the full VLBI resolution ( $13.2 \times 7.2$  mas,  $111 \times 61$  pc), with a  $4\sigma$  point source upper limit of  $26 \mu\text{Jy beam}^{-1}$ , or an upper limit to the intrinsic brightness temperature of  $4.7 \times 10^5$  K. The extent of the observed continuum source at 1.4 GHz and the derived brightness temperature limits are consistent with the radio emission (and thus presumably the far-infrared emission) being powered by a major starburst in GOODS 850–3, with a star formation rate of  $\sim 2500 M_{\odot} \text{ yr}^{-1}$ . Moreover, the absence of any continuum emission at the full resolution of the VLBI observations indicates the lack of a compact radio AGN source in this  $z = 1.87$  SMG.

*Subject headings:* galaxies: individual (GOODS 850–3) — galaxies: active — galaxies: high-redshift — radio continuum: galaxies — techniques: interferometric

---

<sup>b</sup>Department of Physics and Astronomy, University of Hawaii

<sup>c</sup>Institute for Astronomy, University of Hawaii

<sup>1</sup>Based in part on observations obtained at the Canada-France-Hawaii Telescope (CFHT), which is operated by the National Research Council of Canada, the Institut National des Sciences de l’Univers of the Centre National de la Recherche Scientifique of France, and the University of Hawaii, and the Subaru Telescope, which is operated by the National Astronomical Observatory of Japan.

## 1. INTRODUCTION

The strength of the far-infrared (FIR) extragalactic background implies that a large fraction of galaxy formation and black hole accretion activity is hidden by dust (see a review in Lagache, Puget, & Dole 2005). A large fraction ( $\sim 30\%$ ) of the background has been resolved in the submillimeter into discrete high-redshift sources (e.g., Smail, Ivison, & Blain 1997; Hughes et al. 1998; Barger et al. 1998). Bright ( $\gtrsim 5$  mJy at  $850 \mu\text{m}$ ) submillimeter galaxies (SMGs) were found to be mostly at high redshifts of  $z \sim 1.5\text{--}3$ , and they dominate the total star formation in this redshift range (Chapman et al. 2003, 2005). They have total infrared (IR) luminosities of  $10^{12}$  to  $> 10^{13} L_{\odot}$ , corresponding to star formation rates of  $10^2\text{--}10^3 M_{\odot} \text{ yr}^{-1}$ .

An outstanding question about bright SMGs is whether the FIR emission is powered by active galactic nuclei (AGNs) or by starbursts. This has been studied at various wavelengths using X-ray (Alexander et al. 2003, 2005), optical (Barger et al. 1999; Chapman et al. 2005), near-infrared (NIR) (Swinbank et al. 2004), and mid-infrared (MIR) data (Pope et al. 2008; Murphy et al. 2009). At even longer wavelengths, radio and mm interferometers add another powerful way to investigate the existence of AGNs through morphology. A small sample of two SMGs were marginally resolved by the Submillimeter Array at sub-arcsec resolutions, suggesting extended starbursts to be the main power source (Younger et al. 2008). By combining the Multi-Element Radio Linked Interferometer (MERLIN) and the Very Large Array (VLA), Chapman et al. (2004) obtained high angular resolution ( $\sim 0''.3$ ) 1.4 GHz images of 12 SMGs. The majority (8 out of 12; 67%) of their sources were resolved by MERLIN+VLA, again suggesting extended starbursts. However, the resolution of MERLIN+VLA is insufficient to probe radio emission from compact radio AGNs. Whether the remaining 33% of compact radio sources in the MERLIN+VLA sample are powered by compact nuclear starbursts or by AGNs thus remains to be tested.

The high resolution of Very Long Baseline Interferometry (VLBI) observations permits a detailed look at the physical structures in the most distant cosmic sources. Also, sensitive VLBI continuum observations can be used to determine the nature of the energy source(s) in these galaxies at radio frequencies. To date, several high redshift QSOs have been imaged at milliarcsecond resolution (Frey et al. 1997, 2003; Beelen et al. 2004; Momjian et al. 2004, 2005, 2008). These are the highest resolution studies of such distant QSOs by far. Here we are expanding such work on high- $z$  SMGs. In this paper, we present sensitive VLBI observations of the SMG GOODS 850–3.

The source GOODS 850–3 (aka SMM J123618.3+621551, GN6, Chapman et al. 2004;

Pope et al. 2006), which has an optical redshift of  $1.865^2$  (Chapman et al. 2005), is a luminous SMG with  $S_{850\mu\text{m}} = 7.72 \pm 1.02$  mJy (Wang et al. 2004). This object is one of the strongest radio sources among SMGs, and it is designated as a compact source at  $0.3''$  resolution (Chapman et al. 2004, 2005). The flux density of GOODS 850–3 at 1.4 GHz, measured with MERLIN+VLA observations, is  $S_{1.4\text{GHz}} = 151 \pm 11$   $\mu\text{Jy}$ .

Throughout this paper, we assume a flat cosmological model with  $\Omega_m = 0.3$ ,  $\Omega_\Lambda = 0.7$ , and  $H_0 = 70$  km s $^{-1}$  Mpc $^{-1}$ . In this model, and at the distance of GOODS 850–3, 1 milliarcsecond (mas) corresponds to 8.4 pc.

## 2. OBSERVATIONS AND DATA REDUCTION

The VLBI observations of GOODS 850–3 were carried out at 1.4 GHz on 2006 December 9 and 2007 February 13 using the High Sensitivity Array (HSA), which includes the Very Long Baseline Array (VLBA), the phased Very Large Array (VLA), and the Green Bank Telescope (GBT) of the NRAO<sup>3</sup>. Eight adjacent 8 MHz baseband channel pairs were used in the observations, both with right- and left-hand circular polarizations, and sampled at two bits. The data were correlated at the VLBA correlator in Socorro, NM, with a 2 s correlator integration time. The total observing time was 16 hr. In these observations, the shortest baseline is between the phased VLA and the VLBA antenna in Pie Town, NM, which is 52 km. This short-spacing limit filters out all spatial structure larger than about  $0''.42$ . Table 1 summarizes the parameters of these observations.

The observations employed nodding-style phase referencing using the calibrator J1229+6335 ( $S_{1.4\text{GHz}} = 0.38$  Jy) with a cycle time of 280 sec, 200 sec on the target source and 80 sec on the calibrator. The angular separation between the target and the phase calibrator is  $1.55^\circ$ . A number of test cycles were also included to monitor the coherence of the phase referencing. These tests involved switching between two calibrators, the phase calibrator J1229+6335 and the phase-check calibrator J1219+6600 ( $S_{1.4\text{GHz}} = 0.06$  Jy), using a similar cycle time to that used for the target source. The angular separation between these two calibrators is  $2.6^\circ$ .

---

<sup>2</sup>Pope et al. 2008 derived a redshift of  $2.00 \pm 0.03$  from *Spitzer* MIR spectroscopy with PAH features. Our observations in § 4.2 show that GOODS 850–3 is extremely optically faint and therefore the spectroscopic observations of Chapman et al. (2005) might have been made on another galaxy. Nevertheless, the inconsistency between the two redshift measurements does not affect our analysis.

<sup>3</sup>The National Radio Astronomy Observatory is a facility of the National Science Foundation operated under cooperative agreement by Associated Universities, Inc.

The accuracy of the phase calibrator position is important in phase-referencing observations (Walker 1999), as this determines the accuracy of the absolute position of the target source and any associated components. Phase referencing, as used here, is known to preserve absolute astrometric positions to better than  $\pm 0''.01$  (Fomalont 1999).

Data reduction and analysis were performed using the Astronomical Image Processing System (AIPS) of the NRAO. After applying *a priori* flagging, amplitude calibration was performed using measurements of the antenna gain and system temperature for each station. Ionospheric corrections were applied using the AIPS task “TECOR”. The phase calibrator J1229+6335 was self-calibrated in both phase and amplitude and imaged in an iterative cycle.

Images of the phase-check calibrator, J1219+6600, were deconvolved using two different approaches: (a) by applying the phase and the amplitude self-calibration solutions of the phase reference source J1229+6335 (Figure 1a), and (b) by self calibrating J1219+6600 in both phase and amplitude (Figure 1b). The peak surface brightness ratio of the final images from the two approaches gives a measure of the effect of residual phase errors after phase referencing (i.e., ‘the coherence’ due to phase referencing). At all times, the coherence was found to be better than 93%.

The self-calibration solutions of the phase calibrator, J1229+6335, were applied on the target source, GOODS 850–3, which was then deconvolved and imaged at various spatial resolutions by tapering the visibility data.

### 3. RESULTS & ANALYSIS

Imaging the target source at the full resolution of the VLBI array, which is  $13.2 \times 7.2$  mas ( $111 \times 61$  pc,  $PA = -16^\circ$ ), achieved an rms noise level of  $6.5 \mu\text{Jy beam}^{-1}$ , but it did not reveal any continuum component in the field of GOODS 850–3. This indicates the absence of any compact radio continuum emission with flux densities of  $\geq 4\sigma$  or  $26 \mu\text{Jy beam}^{-1}$ , which in turn implies an upper limit to the intrinsic brightness temperature (corresponding to a rest frequency of  $\sim 4$  GHz) of  $4.7 \times 10^5$  K for any compact radio source in GOODS 850–3. Our coherence tests during these observations using two VLBI calibrators show that the lack of a strong point source in GOODS 850–3 at the full resolution of the array cannot be due to the phase referencing procedure. The VLBI flux limit reported above is almost an order of magnitude lower than the flux measured by the VLA+MERLIN ( $151 \pm 11 \mu\text{Jy}$ ) at 1.4 GHz (Chapman et al. 2004). This immediately implies that more than 90% of the radio continuum emission in GOODS 850–3 is extended and not confined to a central AGN.

In the following, we assess whether our HSA observations can recover the flux seen by the VLA and MERLIN. To do so, we applied two dimensional Gaussian tapers on the visibility data with various values. However, the only image with a reliable  $\sim 4\sigma$ , detection was obtained by applying a Gaussian taper falling to 30% at  $0.5 M\lambda$  in both the u- and v-directions. This gave a beam size of  $0''.47 \times 0''.34$  ( $3.9 \times 2.9 \text{ kpc}^2$ , P.A.= $18^\circ$ ). The resulting image is shown in Figure 2. This image is practically made from the shortest baseline in our data set (phased VLA – Pie Town), but only after calibrating its visibilities using all the antennas in the array as described in §2. The rms noise level in this naturally weighted image is  $38 \mu\text{Jy beam}^{-1}$ . At this resolution, a Gaussian model fitting reveals a marginally resolved continuum source with a peak flux density of  $148 \pm 38 \mu\text{Jy beam}^{-1}$  and a total flux density of  $168 \pm 73 \mu\text{Jy}$ , which agrees well with the flux density measured with the VLA+MERLIN at 1.4 GHz (Chapman et al. 2004). Deconvolving the synthesized beam from the Gaussian fitting model of the source results in  $0''.27 \pm 0''.12$  for the size of the major axis, and an upper limit of  $0''.23$  for the size of the minor axis, i.e.,  $0''.27(\pm 0''.12) \times < 0''.23$ , or  $2.3(\pm 1.0) \times < 1.9 \text{ kpc}^2$ . The derived intrinsic brightness temperature limit is  $T_b > (5 \pm 2) \times 10^3 \text{ K}$ .

## 4. DISCUSSION

### 4.1. Radio Properties

We have detected 1.4 GHz emission from GOODS 850–3 (corresponding to a rest-frame frequency of  $\sim 4$  GHz) using the HSA. At a relatively low spatial resolution ( $0''.47 \times 0''.34$ ; Figure 2) the limit on the intrinsic brightness temperature value of the detected continuum source is  $> (5 \pm 2) \times 10^3 \text{ K}$ . Its flux density at this resolution is consistent with that measured with the VLA+MERLIN (Chapman et al. 2004, 2005). This implies that the radio continuum emission at 1.4 GHz is confined to the extent of the structure seen in the VLA+MERLIN image at  $0''.3$  resolution (Chapman et al. 2004), or to the extent of the deconvolved size scale reported in this paper, which is  $0''.27(\pm 0''.12) \times < 0''.23$ , or  $2.3(\pm 1.0) \times < 1.9 \text{ kpc}^2$ .

At the full resolution of our array ( $13.2 \times 7.2 \text{ mas}$ ), the radio emission from GOODS 850–3 is resolved out and does not show any single dominant source of very high brightness temperature ( $< 4.7 \times 10^5 \text{ K}$ ). This is in contrast to the results obtained by Momjian et al. (2004) on a sample of three high- $z$  radio-loud quasars imaged with the VLBA, namely J1053-0016 ( $z = 4.29$ ), J1235-0003 ( $z = 4.69$ ), and J0913+5919 ( $z = 5.11$ ). In each of these  $z > 4$  quasars, a radio-loud AGN dominates the emission at 1.4 GHz on a few mas size scale, with intrinsic brightness temperatures in excess of  $10^9 \text{ K}$ .

Condon et al. (1991) have derived an empirical upper limit to the brightness tempera-

ture for nuclear starbursts. For a frequency value of 4 GHz (our rest frequency), the resulting limit on the intrinsic brightness temperature is  $T_b \leq 4.8 \times 10^4$  K, while typical radio-loud AGNs have brightness temperatures exceeding this value by at least two orders of magnitude. These authors also present a possible physical model for this limit involving a mixed non-thermal and thermal radio emitting (and absorbing) plasma, constrained by the radio-to-FIR correlation for star-forming galaxies. The measured intrinsic brightness temperature limit for the radio source in GOODS 850–3 is consistent with the empirical upper limit value for nuclear starbursts.

For GOODS 850–3, the derived intrinsic brightness temperatures from our VLBI observations are typical of starburst galaxies. However, when compared to local starburst powered Ultra-Luminous IR galaxies (ULIRGs; Sanders & Mirabel 1996), such as Arp 220, Mrk 273, and IRAS 17208–0014 (Smith et al. 1998; Carilli & Taylor 2000; Momjian et al. 2003, 2006; Lonsdale et al. 2006), the radio continuum emission from GOODS 850–3 is an order of magnitude greater in luminosity, but also an order of magnitude larger in extent.

In starburst dominated galaxies, the radio continuum is the sum of supernovae (SNe), supernova remnants, and residual relativistic electrons in the interstellar medium, as shown in the model presented by Condon et al. (1991). However, detecting individual SNe in GOODS 850–3 at  $z = 1.87$  is unlikely. Lonsdale et al. (2006) reported the detection of 49 luminous radio SNe in the prototype ULIRG Arp 220 with flux densities between 0.053 and 1.228 mJy and typical upper limits on their linear extent of less than 1 pc. At the distance of GOODS 850–3, the flux densities of such luminous radio SNe would be between  $(5 - 115) \times 10^{-3} \mu\text{Jy}$ . These values are two to three orders of magnitude lower than the rms noise levels achieved in our VLBI observations.

Our radio continuum results with the HSA clearly rule out a compact radio-loud AGN in GOODS 850–3 and show physical characteristics consistent with an extreme starburst. However, we cannot completely rule out that the radio emission in this source is from a kpc scale radio-jet structure with a very faint compact AGN component that contributes to less than 10% of the total radio continuum emission, and hence falls below our detection threshold at the full resolution of the array. Therefore, we further extend the discussion regarding the nature of the power source(s) in this SMG, and whether it hosts a radio-quiet AGN, by looking into the optical and IR properties of GOODS 850–3 at various bands, as described in the following section.

## 4.2. Multi-wavelength Properties

Evidence for an intensive starburst in GOODS 850–3 is also seen at various other wavelengths. First, Carrilli & Yun (1999) presented a method of using the local radio–FIR correlation and the radio and submillimeter flux densities to estimate redshifts of SMGs. Barger, Cowie, & Richards (2000) derived a simple redshift formula for Arp 220-like Spectral Energy Distribution (SEDs):  $z + 1 = 0.98(S_{850}/S_{1.4})^{0.26}$ . With this formula, the measured redshift  $z = 1.865$ , and the radio and submillimeter fluxes of GOODS 850–3, we find its radio and submillimeter SED to be consistent with Arp 220 within 20%. This implies that this SMG excellently follows the same radio–FIR correlation as Arp 220, and suggests that its FIR emission is powered by a starburst.

GOODS 850–3 is among the first SMGs with an X-ray detection (Alexander et al. 2003). It is detected at soft X-rays in the 2Ms *Chandra* image of the Chandra Deep Field-North (CDFN), but it is not detected at hard X-rays. It has an X-ray luminosity of  $\sim 0.5 \times 10^{42}$  erg s<sup>-1</sup>. These authors suggested that this source is powered by star formation, but they did not rule out a highly obscured AGN with low X-ray luminosity.

Pope et al. (2008) obtained a MIR spectrum on GOODS 850–3 (GN06 in their paper) and decomposed the spectrum into PAH and “continuum” components. The continuum component contributes  $\sim 50\%$  to its MIR luminosity, and such a component can be powered by a dusty AGN. The MIR spectral decomposition method was further refined by Murphy et al. (2009), who noted that such MIR continuum fraction is a strict upper limit on the AGN contribution at this wavelength band. However, AGN dust components are warmer than those powered by starbursts and contribute mainly to the MIR. We therefore expect the AGN fraction in the total IR luminosity of GOODS 850–3 to be negligible.

None of the above observational evidence, including our HSA observations, absolutely rule out the existence of an obscured AGN in GOODS 850–3. However, a kpc-scale starburst is consistent with all observations from the X-ray to the radio.

The last piece of evidence comes from the optical and NIR morphologies. For the optical, we combined the latest version of the four (F435W, F606W, F775W, and F850LP) *HST* ACS images from The Great Observatories Origins Deep Survey (GOODS; Giavalisco et al. 2004) to form a deep “white” optical image for GOODS 850–3. For the NIR, we used three sets of data. First, Lihwai Lin et al. (in preparation) obtained nearly 30 hr of GOODS-N imaging data at *J*-band with the Wide-Field Infrared Camera (WIRCam) on the 3.6 m Canada-France-Hawaii Telescope (CFHT). We downloaded these *J*-band data from the public archive and reduced them. We also used the WIRCam on CFHT to obtain a deep *K<sub>S</sub>*-band image with nearly 50 hr of integration. Lastly, we obtained a deep *K<sub>S</sub>*-band image of the GOODS-N



with the Multi-Object Infrared Camera and Spectrograph (MOIRCS) on the 8.2 m Subaru Telescope. This MOIRCS imaging is described in Wang, Barger, & Cowie (2009a). In this imaging, GOODS 850–3 received approximately 4 hr of integration. All the above  $J$ - and  $K_S$ -band images are still being deepened by various groups. All the data reduction was carried out by our group using SIMPLE Imaging and Mosaicking Pipeline (SIMPLE<sup>4</sup>, Wang et al. 2009b). More details about the  $K_S$ -band observations and data reduction can be found in Barger, Cowie, & Wang (2008) and Wang et al. (2009b). The reduction of the  $J$ -band data is identical to that of the  $K_S$ -band. Here we adopt the MOIRCS  $K_S$ -band image for morphological analyses because of its high angular resolution (FWHM  $\sim 0''.4$ ), and the WIRCam  $K_S$ -band image for photometry because of its greater depth.

We present the ultradeep ACS white, WIRCam  $J$ , and MOIRCS  $K_S$  images of GOODS 850–3 in Figure 3, and the F435W to 8.0  $\mu\text{m}$  photometry in Table 2. The ACS fluxes were measured with  $d = 0''.8$  apertures at the location of the  $K_S$  source. This is the maximum possible aperture size for the ACS fluxes to be free of contamination from nearby objects. The  $J$ -band image does not have sufficient resolution to separate GOODS 850–3 from nearby objects, and therefore we did not attempt to measure its  $J$ -band flux. The  $K_S$ -band flux is measured with SExtractor (Bertin & Arnouts 1996) “AUTO” aperture, which approximates its total flux. In addition, Wang et al. (2009b) used a CLEAN-like method to construct *Spitzer* IRAC source catalogs based on the WIRCam  $K_S$  image. We include their IRAC fluxes for GOODS 850–3 in Table 2. We present the observed optical to IRAC SED in Figure 4.

GOODS 850–3 is extremely faint in the optical, undetected by even the combination of the four ACS images (also see Chapman et al. 2004). It shows some hint of flux at F850LP (see Table 2) but nothing appears visually in the F850LP image and the white image. It clearly shows up at  $J$ -band, however it is blended with a nearby galaxy. In the  $K_S$ -band and *Spitzer* images, GOODS 850–3 is the brightest galaxy in its neighborhood. With the excellent,  $0''.4$ , resolution of Subaru at  $K_S$ -band, the stellar component of GOODS 850–3 is resolved. A simple Gaussian fit to the source in this  $K_S$ -band image gives a FWHM of  $1''.03 \times 0''.63$ , corresponding to  $8.7 \times 5.3 \text{ kpc}^2$  at its redshift. The image shows an elongated morphology, which may be indicative of an edge on rotating disk, and a pronounced central region that coincides with the radio position, but does not dominate the total  $K_S$  luminosity. These are consistent with a nuclear starburst hosted by a massive galaxy.

The above optical and near-IR observations imply a large galaxy of roughly 9 kpc in size that is entirely hidden by dust. This shows that dense molecular clouds are widely

---

<sup>4</sup>also see [http://www.asiaa.sinica.edu.tw/~sim\\$whwang/idl/SIMPLE](http://www.asiaa.sinica.edu.tw/~sim$whwang/idl/SIMPLE)

distributed in this galaxy, despite the fact that only its nucleus is actively forming stars.

### 4.3. Star Formation Rate and Surface Density

The results obtained from various bands in the electromagnetic spectrum (radio to the X-ray) suggest that the dominant power source in the SMG GOODS 850–3 is a starburst. Therefore, in the following, we derive an estimate of its star formation rate and star formation surface density.

The 850  $\mu\text{m}$  flux density of GOODS 850–3 implies a total IR luminosity of  $1.5 \times 10^{13} L_{\odot}$  ( $L_{\text{IR}} = 1.9 \times 10^{12} S_{850\mu\text{m}} L_{\odot} \text{ mJy}^{-1}$ ; Blain et al. 2002). Assuming that this IR luminosity is entirely powered by a starburst, then the associated star formation rate (SFR) is  $\sim 2500 M_{\odot} \text{ yr}^{-1}$  for a Salpeter initial mass function ( $\text{SFR}(M_{\odot} \text{ yr}^{-1}) = 1.7 \times 10^{-10} L_{\text{IR}}(L_{\odot})$ ; Kennicutt 1998). An estimate of the SFR can also be calculated using the conversion factor between radio luminosity and SFR ( $\text{SFR}(M_{\odot} \text{ yr}^{-1}) = 5.9 \times 10^{-22} L_{1.4\text{GHz}}(\text{W Hz}^{-1})$ ; Yun, Reddy, & Condon 2001), which is derived using the local radio–FIR correlation. The radio luminosity of GOODS 850–3 is  $3.7 \times 10^{24} \text{ W Hz}^{-1}$ , and the resulting SFR is  $\sim 2200 M_{\odot} \text{ yr}^{-1}$ . The consistency in the SFR values derived from the radio and the IR luminosities simply confirms that this SMG follows the local radio–FIR correlation. Moreover, this suggests that the star formation activity is well confined within the radio source detected in our HSA observations.

The size of the source seen in our 1.4 GHz image (Figure 2) compares well with other SMGs, but is considerably smaller than optically selected starbursting galaxies at high redshift (see, e.g., Bouché et al. 2007). From the size and the SFR of this SMG, we derive a star formation rate surface density of  $\Sigma_{\text{SFR}} \sim 700 M_{\odot} \text{ yr}^{-1} \text{ kpc}^{-2}$ . This surface density is extremely high even after including the  $\sim 40\%$  uncertainty in its size. For instance, the derived  $\Sigma_{\text{SFR}}$  in GOODS 850–3 is a few times larger than that seen in a sample of SMGs imaged at millimeter wavelengths (Tacconi et al. 2006). Such a high value is at the very high end of SMGs (see Figure 3 of Bouché et al. 2007), and is comparable to that measured in the two extremely luminous SMGs resolved by high resolution submillimeter observations (Younger et al. 2008). Furthermore, the  $\Sigma_{\text{SFR}}$  in GOODS 850–3 is comparable to that measured in the host galaxy of the  $z = 6.42$  QSO SDSS J114816.64+525150.3 (Walter et al. 2009). Such high  $\Sigma_{\text{SFR}}$  values are consistent with recent theoretical descriptions of (dust opacity) Eddington limited star formation of a radiation pressure-supported starbursts on kpc scales (Thompson et al. 2005).

Using the population synthesis model of Bruzual & Charlot (2003), the Hyperz package

(Bolzonella, Miralles, & Pelló 2000) package, and the ACS,  $K_S$ , and IRAC photometry in Table 2, we find a stellar mass of  $1.4 \times 10^{11} M_\odot$  in GOODS 850–3. The best-fit SED is shown in Figure 4. With a star formation rate of  $\sim 2500 M_\odot \text{ yr}^{-1}$ , the stellar mass can be doubled in just 56 Myr, roughly 1.6% of its Hubble time. The model also requires an extinction of  $A_V \sim 2.8$  to explain the nondetections in the optical bands. We expect the extinction in the nuclear starburst component to be even larger. Furthermore, we derive a value of  $18 \text{ Gyr}^{-1}$  for the star-formation rate per unit stellar mass (i.e., specific star-formation rate; SSFR) in GOODS 850–3. This is an order of magnitude higher than that seen in normal star forming galaxies at  $z \sim 2$ , which have SSFR values of about  $2 - 3 \text{ Gyr}^{-1}$  (Pannella et al. 2009).

In summary, GOODS 850–3 has a kpc-scale nuclear starburst with a star formation rate of  $\sim 2500 M_\odot \text{ yr}^{-1}$ . No evidence of an AGN is seen at any wavelength. An upper limit on its MIR AGN contribution of 50% is estimated by Pope et al. (2008), but the AGN contribution to its total IR luminosity should be much lower. Moreover, our HSA observations reveal that more than 90% of the radio continuum emission in this source is extended and not confined to a central compact AGN. GOODS 850–3 has a stellar component of  $1.4 \times 10^{11} M_\odot$  with a spatial extent of roughly 9 kpc. This huge and massive stellar component is entirely hidden by dust, suggesting an extremely rich molecular gas reservoir fueling the nuclear starburst.

## 5. ACKNOWLEDGMENTS

This research made use of the NASA/IPAC Extragalactic Database (NED), which is operated by the Jet Propulsion Laboratory, California Institute of Technology, under contract with the National Aeronautics and Space Administration. This work was initiated when WHW was a Jansky Fellow at NRAO. WHW acknowledges the great support from the NRAO, and LLC and AJB acknowledge support from NSF grants AST 0709356 and AST 0708793, respectively.

## REFERENCES

- Alexander, D. M., Bauer, F. E., Brandt, W. N., Hornschemeier, A. E., Vignali, C., Garmire, G. P., Schneider, D. P., Chartas, G., & Gallagher, S. C. 2003, *AJ*, 125, 383
- Alexander, D. M., Bauer, F. E., Chapman, S. C., Smail, I., Blain, A. W., Brandt, W. N., & Ivison, R. J. 2005, *ApJ*, 632, 736
- Barger, A. J., Cowie, L. L., Sanders, D. B., Fulton, E., Taniguchi, Y., Sato, Y., Kawara, K., & Okuda, H. 1998, *Nature*, 394, 248
- Barger, A. J., Cowie, L. L., Smail, I., Ivison, R. J., Blain, A. W., & Kneib, J.-P. 1999, *AJ*, 117, 2656
- Barger, A. J., Cowie, L. L., & Richards, E. A. 2000, *AJ*, 119, 2092
- Barger, A. J., Cowie, L. L., & Wang, W.-H. 2008, *ApJ*, 689, 687
- Beelen, A., Cox, P., Pety, J., Carilli, C. L., Bertoldi, F., Momjian, E., Omont, A., Petitjean, P., Petric, A. O., 2004, *A&A*, 423, 441
- Bertin, E., & Arnouts, S. 1996, *A&A*, 117, 393
- Blain, A. W., Smail, I., Ivison, R. J., Kneib, J.-P., & Frayer, D. T. 2002, *Phys. Rep.*, 369, 111
- Bolzonella, M., Miralles, J.-M., & Pelló, R. 2000, *A&A*, 363, 476
- Bouché, N., et al. 2007, *ApJ*, 671, 303
- Bruzual, G., & Charlot, S. 2003, *MNRAS*, 344, 1000
- Carilli, C. L., & Yun, M. S. 1999, *ApJ*, 513, L13
- Carilli, C. L., & Taylor, G. B. 2000, *ApJ*, 532, L95
- Chapman, S. C., Blain, A. W., Ivison, R. J., & Smail, I. R. 2003, *Nature*, 422, 695
- Chapman, S. C., Smail, I., Windhorst, R., Muxlow, T., Ivison, R. J. 2004, *ApJ*, 611, 732
- Chapman, S. C., Blain, A. W., Smail, Ian, Ivison, R. J. 2005, *ApJ*, 622, 772
- Condon, J. J., Huang, Z. -P., Yin, Q. F., & Thuan, T. X. 1991, *ApJ*, 378, 65
- Fomalont, E. B. 1999, in *Synthesis Imaging in Radio Astronomy II*, ed. G.B. Taylor, C. L. Carilli, & R. A. Perley (San Francisco: ASP), 301

- Frey, S., Gurvits, L. I., Kellermann, K. I., Schilizzi, R. T., & Pauliny-Toth, I. I. K. 1997, *A&A*, 325, 511
- Frey, S., Mosoni, L., Paragi, Z., & Gurvits, L. I. 2003, *MNRAS*, 343, L20
- Giavalisco, M., et al. 2004, *ApJ*, 600, L93
- Hughes, D. H., et al. 1998, *Nature*, 394, 241
- Kennicutt, R. C. 1998, *ARA&A*, 36, 189
- Lonsdale, C. J., Diamond, P. J., Thrall, H., Smith, H. E., Lonsdale, C. J. 2006, *ApJ*, 647, 185
- Lagache, G., Puget, J.-L., & Dole, H. 2005, *ARA&A*, 43, 727
- Momjian, E., Romney, J. D., Carilli, C. L., Troland, T. H., & Taylor, G. B. 2003, *ApJ*, 587, 160
- Momjian, E., Petric, A. O., & Carilli, C. L. 2004, *AJ*, 127, 587
- Momjian, E., Carilli, C. L., Petric, A. O. 2005, *AJ*, 129, 1809
- Momjian, E., Romney, J. D., Carilli, C. L., & Troland, T. H. 2006, *ApJ*, 653, 1172
- Momjian, E., Carilli, C. L., McGreer, I. 2008, *AJ*, 136, 344
- Murphy, E. J., Chary, R.-R., Alexander, D. M., Dickinson, M., Magnelli, B., Morrison, G., Pope, A., & Teplitz, H. I. 2009, *ApJ*, 698, 1380
- Pannella, M., et al. 2009, *ApJ*, 698, 116
- Pope, A., et al. 2006, *MNRAS*, 370, 1185
- Pope, A., et al. 2008, *ApJ*, 675, 1171
- Sanders, D. B., & Mirabel, I. F. 1996, *ARA&A*, 34, 749
- Smail, I., Ivison, R. J., & Blain, A. W. 1997, *ApJ*, 490, L5
- Smith, H. E., Lonsdale, C. J., Lonsdale, C. J., & Diamond, P. J. 1998, *ApJ*, 493, L17
- Swinbank, A. M., Smail, I., Chapman, S. C., Blain, A. W., Ivison, R. J., & Keel, W. C. 2004, *ApJ*, 617, 64
- Taccono, L. J., et al. 2006, *ApJ*, 640, 228

- Thompson, T. A., Quataert, E., & Murray, N., 2005, *ApJ*, 630, 167
- Walker, C. R. 1999, in *Synthesis Imaging in Radio Astronomy II*, ed. G.B. Taylor, C. L. Carilli, & R. A. Perley (San Francisco: ASP), 433
- Walter, F., et al. 2009, *Nature*, 457, 699
- Wang, W.-H., Cowie, L. L., Barger, A. J. 2004, *ApJ*, 613, 655
- Yun, M. S., Reddy, N. A., & Condon, J. J. 2001, *ApJ*, 554, 803
- Wang, W.-H., Barger, A. J., & Cowie, L. L. 2009, *ApJ*, 690, 319
- Wang, W.-H., et al. 2009, in preparation
- Younger, J. D., et al. 2008, *ApJ*, 668, 59

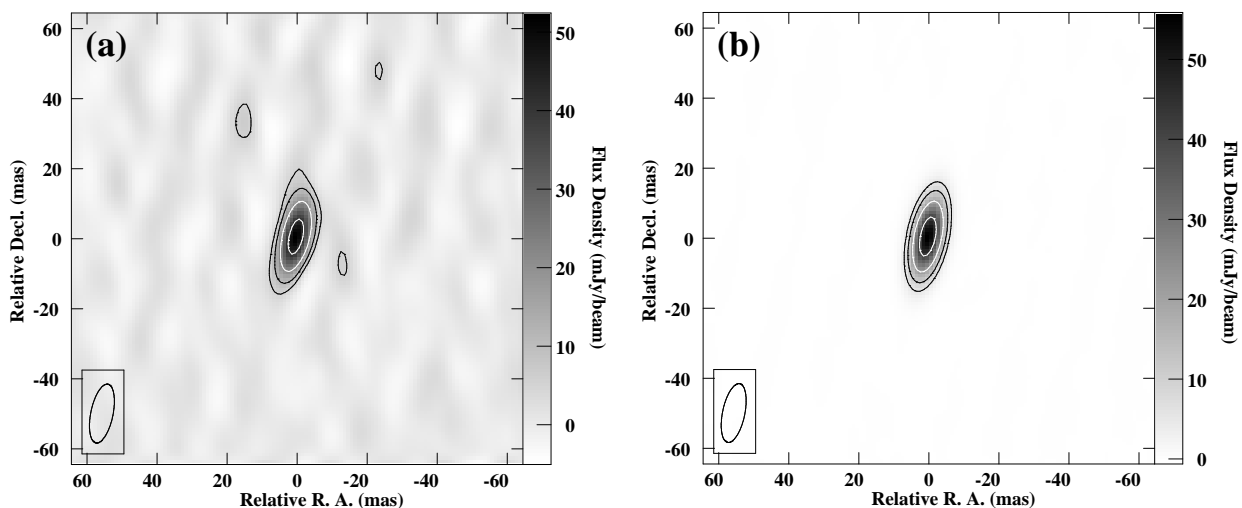


Fig. 1.— Continuum images of the phase-check calibrator J1219+6600 at 1.4 GHz: a) obtained by applying the phase and the amplitude self-calibration solutions of the phase reference source J1229+6335, b) obtained by self calibrating J1219+6600 itself, in both phase and amplitude. The restoring beam size in both images is  $17.1 \times 6.4$  mas in position angle  $-12^\circ$ . The contour levels are at  $-3, 3, 6, 12, 24$  times the rms noise level in the phase-referenced image (left), which is  $1.71 \text{ mJy beam}^{-1}$ . The gray-scale range is indicated at the right side of each image. The reference point  $(0, 0)$  in both images is  $\alpha(\text{J2000.0}) = 12^{\text{h}}19^{\text{m}}35^{\text{s}}.7941$ ,  $\delta(\text{J2000.0}) = +66^\circ00'31''.845$ .

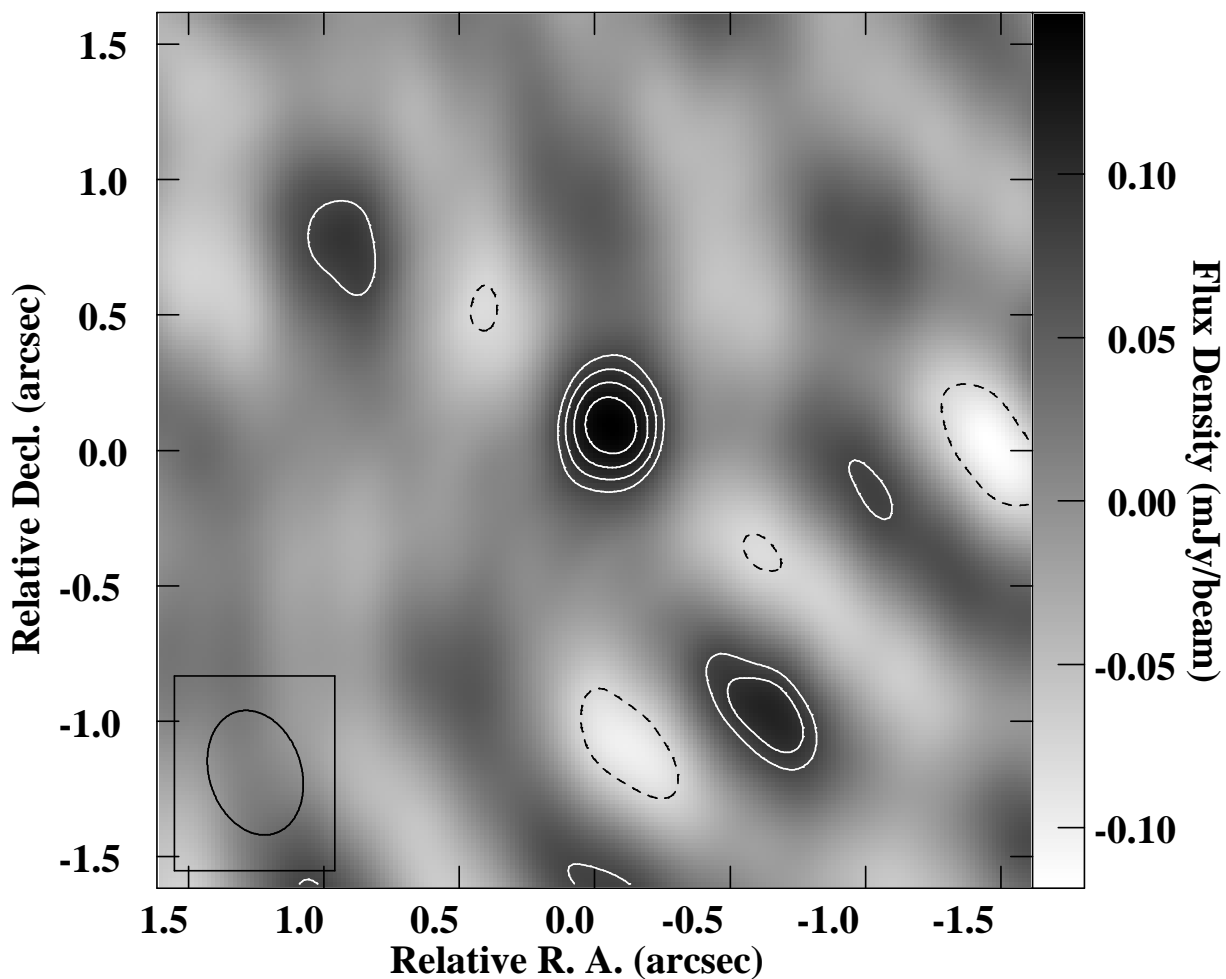


Fig. 2.— Naturally weighted 1.4 GHz continuum image of GOODS 850–3 at  $0.47'' \times 0.34''$  resolution (P.A.= $18^\circ$ ). The peak flux density is  $148 \mu\text{Jy beam}^{-1}$ , and the contour levels are at  $-2, 2, 2.5, 3, 3.5$  times the rms noise level, which is  $38 \mu\text{Jy beam}^{-1}$ . The gray-scale range is indicated at the right side of the image. The reference point (0, 0) is  $\alpha(\text{J2000.0}) = 12^{\text{h}}36^{\text{m}}18^{\text{s}}3317$ ,  $\delta(\text{J2000.0}) = +62^\circ15'50''.608$ . A two dimensional Gaussian taper falling to 30% at  $0.5 \text{ M}\lambda$  was applied.



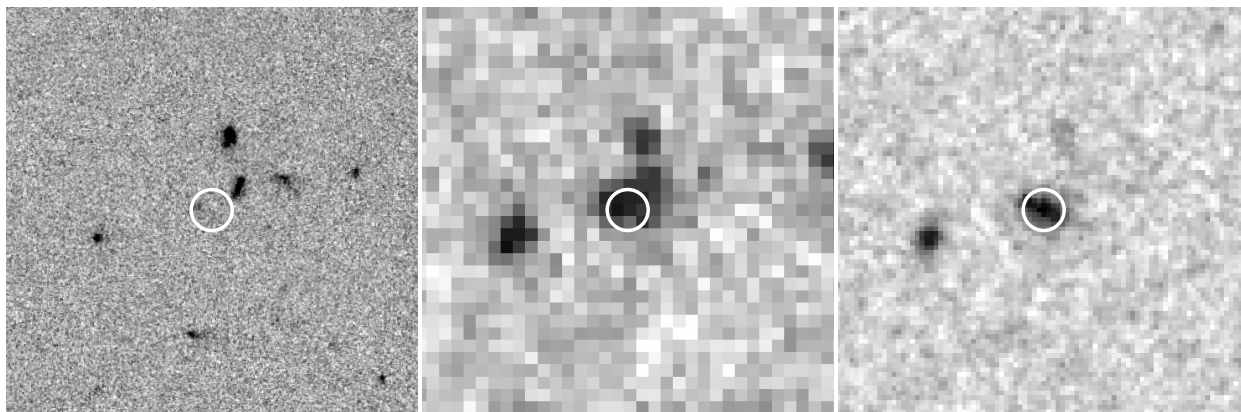


Fig. 3.— Optical and near-IR images of GOODS 850–3. From left are the *HST* ACS “white” image (F435W+F606W+F775W+F850LP), the CFHT *J*-band image, and the Subaru *K<sub>S</sub>*-band image. All panels have 10'' sizes and north is up. Circles indicate the 1.4 GHz position and have 1'' diameters. Note that GOODS 850–3 entirely disappears in the optical but becomes very bright at longer wavelengths.

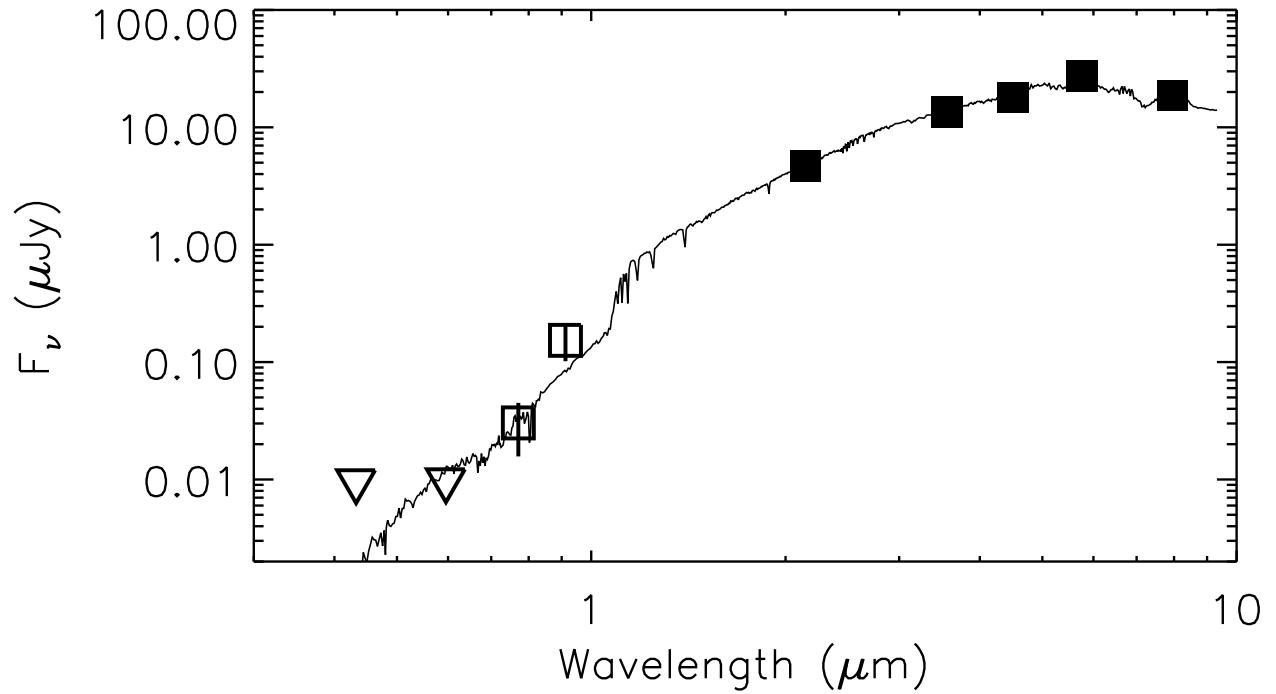


Fig. 4.— The SED of GOODS 850–3. Symbols show the observed data in Table 2. Filled squares are detections. Open squares are low significance flux measurements. Downward triangles are  $1\sigma$  upper limits. The curve is the best-fit SED from the Bruzual & Charlot (2003) models, which has a continuous starburst of 0.36 Gyr, extinction of  $A_V = 2.8$ , and a stellar mass of  $1.4 \times 10^{11} M_\odot$ .

Table 1. PARAMETERS OF THE VLBI OBSERVATIONS OF GOODS 850–3

Parameters	Values
Observing Dates .....	2006 Dec. 9 & 2007 Feb. 13
Total observing time (hr) .....	16
Phase calibrator .....	J1229+6335
Phase-referencing cycle time (sec)	280
Frequency (GHz) .....	1.4
Total bandwidth (MHz) .....	64

Table 2. OPTICAL TO MID-INFRARED PHOTOMETRIC DATA OF GOODS 850–3

Wave Band	Flux ( $\mu\text{Jy}$ )
ACS F435W	$0.012 \pm 0.010$
ACS F606W	$0.008 \pm 0.010$
ACS F775W	$0.030 \pm 0.015$
ACS F850LP	$0.153 \pm 0.051$
WIRCam $K_s$	$4.71 \pm 0.14$
IRAC 3.6 $\mu\text{m}$	$13.4 \pm 0.2$
IRAC 4.5 $\mu\text{m}$	$17.9 \pm 0.2$
IRAC 5.8 $\mu\text{m}$	$27.3 \pm 0.6$
IRAC 8.0 $\mu\text{m}$	$18.5 \pm 0.6$